Activity-based protein profiling of diacylglycerol lipases

Baggelaar, M.P.

CHAPTER 4

A highly Selective, Reversible Inhibitor Identified by Comparative Chemoproteomics Modulates Diacylglycerol Lipase Activity in Neurons*

Introduction

Endocannabinoids are endogenous signaling lipids that activate the cannabinoid CB_1 and CB_2 receptor. They play an essential role in human health and disease, regulating processes, such as immunomodulation, energy balance and neurotransmission.[1] There are two main endocannabinoids: anandamide and 2-arachidonoylglycerol (2-AG).[2-4] Both endocannabinoids are often found together, but their levels vary between species, tissue type, developmental stage and pathological condition.[5] Although selective inhibitors of their metabolic pathways have provided information about the biological function of the endocannabinoids, it is still unclear to a large extent which endocannabinoid is responsible for specific cannabinoid CB_1 receptor dependent (patho)physiological effects.[6,7] Selective inhibition of the formation of anandamide and 2-AG would be instrumental to determine which endocannabinoid is responsible for specific CB_1-mediated physiological effects. However, pathway-selective inhibitors for 2-AG and anandamide biosynthesis are currently lacking.

2-AG is mainly formed by the action of two diacylglycerol lipases (DAGL-α and DAGL-β).[8] DAGLs are intracellular, multi-domain integral membrane proteins. The DAGLs share extensive homology, but differ in size: ~120 and ~70 kDa for DAGL-α and DAGL-β respectively.[8,9]

* Baggelaar, M. P.; Chameau, P. J.; Kantae, V.; Hummel, J.; Hsu, K. L.; Janssen, F. J.; van der Wel, T.; Soethoudt, M.; Deng, H.; den Dulk, H.; Allarà, M.; Florea, B. I.; Di Marzo, V.; Wadman, W. J.; Kruse, C. G.; Overkleeft, H. S.; Hankemeier, T.; Werkman, T. R.; Cravatt, B. F.; van der Stelt, M.; Highly Selective, Reversible Inhibitor Identified by Comparative Chemoproteomics Modulates Diacylglycerol Lipase Activity in Neurons. *J. Am. Chem. Soc.* **2015**, *137*, 8851–8857

DAGLs belong to the class of serine hydrolases that employ the typical Ser-His-Asp catalytic triad to hydrolyze the ester bond of acyl chains from arachidonate-containing diacylglycerols in a *sn*-1 specific manner. Studies with DAGL knock-out mice have shown that DAGL-α controls to a large extent the formation of 2-AG in the central nervous system, whereas DAGL-β appears to partake in 2-AG production in the periphery during inflammation.[5,10] Importantly, also basal anandamide levels were reduced in DAGL-α knock-out mice. Selective inhibitors for DAGLs, which can be used in an acute and temporal fashion and do not modulate anandamide levels, would, therefore, constitute an important counterpart of the DAGL knock-out mice, and allow the examination of acute versus congenital inhibition.

Although, several classes of DAGL inhibitors have been described in literature,[8,11-15] these inhibitors are based on the natural substrates and/or have reactive chemical warheads, and are not selective over other serine hydrolases that modulate endocannabinoid signaling (e.g. α,β-hydrolase domain-containing protein 6 and 12 (ABHD6 and ABHD12), monoacylglycerol lipase (MAGL) or fatty acid amide hydrolase (FAAH)). Therefore highly selective DAGL inhibitors are needed to study the cellular role of the biosynthetic enzymes.

Activity-based protein profiling (ABPP) has emerged as a powerful technique for discovering selective enzyme inhibitors acting in their native physiological context.[16] ABPP hinges on the use of activity-based probes (ABPs) to report on enzyme activity in cells, tissue or animals.[17] An ABP normally consists of a covalent, irreversible enzyme inhibitor featuring a reporter entity (fluorophore, biotin, bioorthogonal tag) to label the active site of the enzyme or enzyme family at hand. ABPP is unique in its ability to rapidly identify inhibitor activity and selectivity within large enzyme families in complex proteome samples. The prototypical ABP for serine hydrolases is based on a fluorophosphonate (FP)-warhead.[18] However, this probe does not recognize DAGL-α and the signals for MAGL and ABHD6 cannot be unequivocally established because not all gel bands can be clearly resolved in the brain proteome.[19] The design, synthesis and characterization of a specific β-lactone-containing ABP (MB064) for the detection of DAGL-α activity was described in Chapter 3.[20,21] Using this ABP, 1-(oxazolo[4,5-b]pyridin-2-yl)-6-phenylhexan-1-one (LEI104, Figure 1) was identified as DAGL-α inhibitor. This inhibitor belongs to the class of α-ketoheterocycles and is the first reversible inhibitor for DAGL-α. LEI104 was, however, weakly active in a cellular assay and not selective over FAAH, the enzyme responsible for the metabolism of the other endocannabinoid anandamide (AEA).[22,23] Moreover, activity of LEI104 on DAGL-α was not studied, but in view of the high homology between DAGL-α and DAGL-β it is likely that there is cross-reactivity. To apply α-ketoheterocycles as chemical tools to study 2-AG signaling, it is important to increase their cellular activity, to have selectivity over FAAH and to assess their activity on endogenous DAGL-β.

Here, a structure-guided approach to optimize LEI104, employing a homology-model of DAGL-α is reported. In addition, it was discovered that the β-lactone probe MB064 could also label DAGL-β in cells and tissues. Using these tools LEI105 was characterized as a cellular active, dual DAGL-α/β inhibitor. Comparative chemoproteomics revealed that LEI105 is selective for DAGL-α/β over ABHD6, ABHD12, MAGL and FAAH. Furthermore, targeted lipidomics revealed that LEI105 is able to reduce 2-AG levels in a concentration dependent manner in neuronal cells without affecting AEA levels. With LEI105 cannabinoid CB_1-receptor-dependent short-term synaptic plasticity in a hippocampal slice model can be reduced. In summary, comparative and competitive chemoproteomics was applied to characterize the most selective DAGL inhibitor to date. This inhibitor can be used to study DAGL function in an acute and temporal manner in a neuronal context.

Results & discussion

Structure-guided modeling to identify LEI105 as DAGL-α inhibitor

Previously, the α-ketoheterocycle, 1-(oxazolo[4,5-*b*]pyridin-2-yl)-6-phenylhexan-1-one (LEI104, Figure 1A) was identified as an inhibitor of DAGL-α. To improve the potency of LEI104 a structure-guided modeling approach was used. The binding pose of LEI104 in DAGL-α was investigated in detail using a molecular dynamics simulation in a previously generated homology model.[21] From this analysis, an additional hydrophobic pocket close to the catalytic site that did not appear to be occupied by LEI104 was identified (Figure 1B). Introduction of a phenyl substituent at the 6-position of the oxazolopyridine allowed probing this pocket with the aim of increasing potency and/or selectivity. A α-ketoheterocycle with a para-toluyl group at the 6-position of LEI104 was synthesized and termed LEI105. The synthesis of LEI105 is depicted in scheme 1.

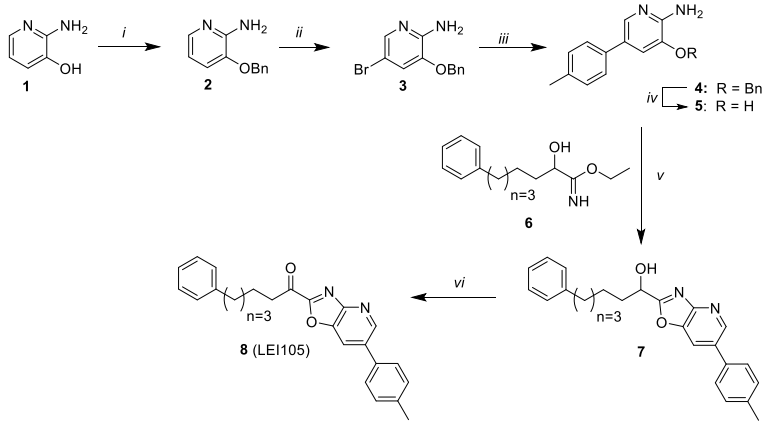

Scheme 1. Synthesis of LEI105. *i)* BnBr, Cs_2CO_3, DMF. *ii)* NBS, ACN, 0 °C. *iii)* 4-methylphenylboronic acid, Pd(dppf)Cl_2, DME/H_2O (20:1). *iv)* Pd/C, MeOH. *v)* EtOH, pyridine, 80 °C, microwave. *vi)* Dess-Martin periodinane, CH_2Cl_2.

Compound **2** was obtained by benzylation of 1-amino-2-hydroxypyridine **1**. The benzyl protection of the alcohol was required in the next step for a high yielding selective bromination in the para position with respect to the amine. The bromination was performed using *N*-bromosuccinimide and resulted in aromatic building block **3**. This compound was used to couple *p*-tolylboronic acid by a Suzuki cross coupling. Subsequent removal of the benzyl protecting group provided building block **5**. The Suzuki cross coupling was performed before the alcohol was deprotected, because the cross coupling with the free alcohol resulted in poor yields. 1-Amino-2-hydroxypyridine **5** was coupled to imidate **6** (synthesized as described in Chapter 3), which resulted in alcohol **7**. Oxidation of **7** using Dess-Martin periodinane afforded final α-ketoheterocycle **8** (LEI105).

The activity of LEI105 was tested on human DAGL-α in a colorimetric assay using *para*-nitrophenylbutyrate as a surrogate substrate.[24] LEI105 proved to be a potent inhibitor with a pIC_{50} of 8.5 ± 0.06 (N=2, n=2), thus some 10-fold more potent than LEI104 (7.4 ± 0.05; N=2, n=2).[21] To confirm that LEI105 was also able to block conversion of the natural substrate 1-stearoyl-2-arachidonoyl-*sn*-glycerol of DAGL-α to the endocannabinoid 2-AG, the real-time fluorescence-based assay was employed.[25] In this assay LEI105 inhibited recombinant human DAGL-α with a pIC_{50} of 7.9 ± 0.08 (N=2, n=2) (Figure 1E), which is a 40-fold increase compared to LEI104 (pIC_{50} 6.3 ± 0.1 (N=2, n=2)). The inhibitory activity of LEI105 was confirmed in a radiometric assay using 1-[^{14}C]oleoyl-2-arachidonoyl-*sn*-glycerol (1.0 mCi mmol^{-1}, 20 μm) as substrate (pIC_{50} of 6.6; n = 2).[8]

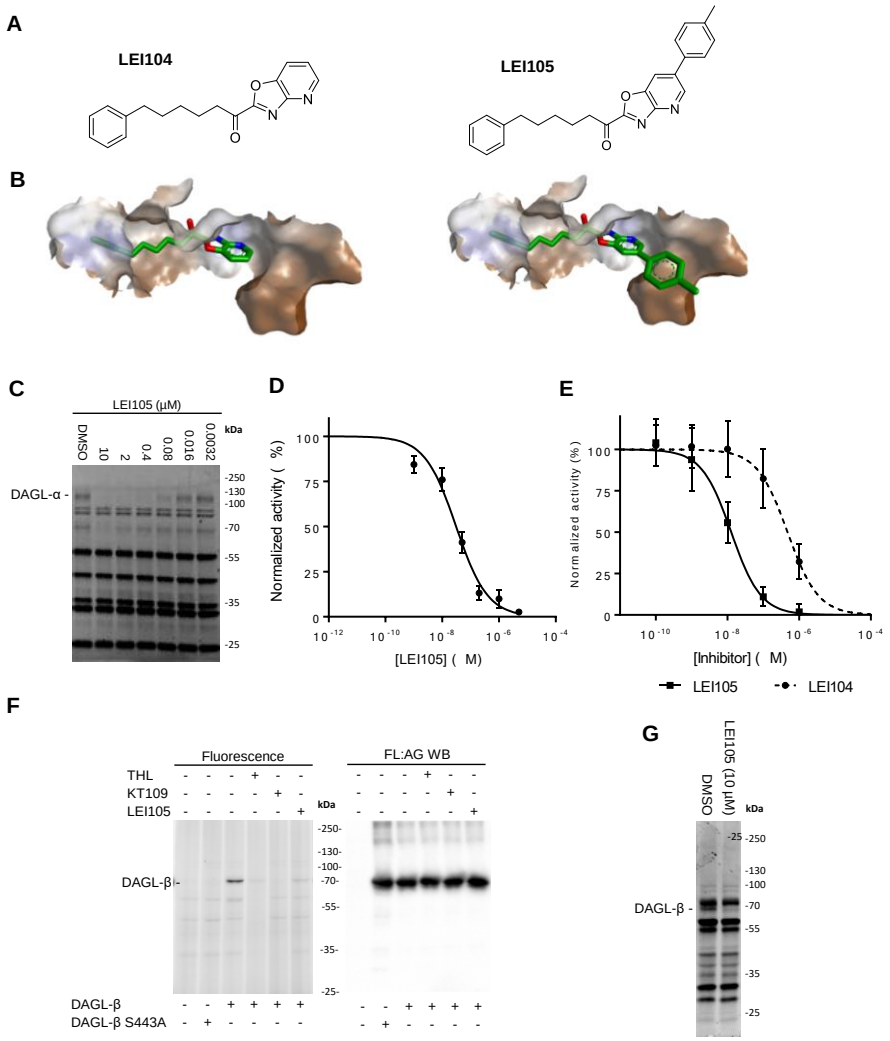

Figure 1. Structure-guided modeling and biochemical characterization of LEI105. *(A)* Structures of α-ketoheterocycle based DAGL inhibitors LEI104 and LEI105. *(B)* LEI104 and LEI105 in a homology model of DAGL-α. *(C)* Representative fluorescent ABPP gel showing dose dependent inhibition of MB064 (250 nM) labeling of endogenous DAGL-α labeling by LEI105 in the mouse brain membrane proteome. (* = DAGL-α breakdown product). *(D)* Dose response curve of DAGL-α inhibition as determined with competitive ABPP (pIC_{50} 7.5 ± 0.07 (IC_{50} = 32 nM); *n* = 3). *(E)* Dose response curve of DAGL-α inhibition by LEI104 (pIC_{50} 6.3 ± 0.1 (IC_{50} = 501 nM); N=2, n=2) and LEI105 (pIC_{50} 7.9 ± 0.08 nM (IC_{50} = 13 nM); N=2, n=2) as determined with a glycerol based natural substrate assay. *(F)* ABPP using MB064 (1 µM) with different hDAGL-β constructs and anti-FLAG western blot of the same gel. *(G)* Competitive ABPP in the mouse spleen membrane proteome using MB064 (1.0 µM) in competition with LEI105 (10 µM), LEI105 can block labeling of endogenously expressed DAGL-β in the mouse spleen membrane proteome.

Determining endogenous DAGL activity using MB064 as ABP

To test the activity of LEI105 on endogenously expressed DAGL-α in mouse membrane proteome, a previously reported ABPP method with MB064 was used.[21] A competitive concentration response experiment with LEI105 in the mouse brain membrane proteome using MB064 revealed a pIC_{50} of 7.5 ± 0.07 (n=3) against DAGL-α (Figure 1C, D).

In view of the high homology between DAGL-α and DAGL-β the activity of LEI105 was also assessed on native DAGL-β. To this end, it was tested whether ABP MB064 was also able to label DAGL-β. MB064 was incubated with membranes from mock and hDAGL-β transfected HEK293T cells. MB064 labeled a protein at the expected molecular weight of DAGL-β, which was not present in the control membranes, or in S443A-hDAGL-β transfected cells, in which the catalytic serine is replaced by alanine using site-directed mutagenesis (Figure 1F). Thus, MB064 can also detect DAGL-β. Labeling of hDAGL-β was inhibited by LEI105 with a pIC_{50} of 7.4 ± 0.07 (n=3) (Figure 2).

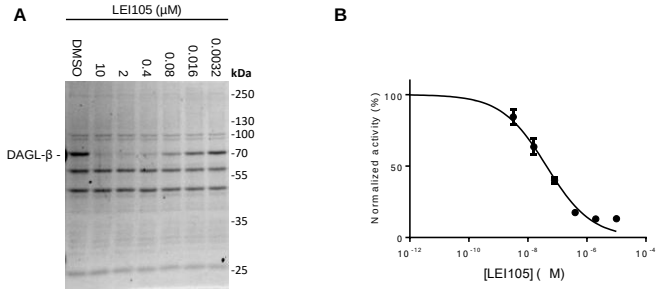

Figure 2. Dose-response of LEI105 as determined by competitive ABPP using ABP MB064 (1 µM) against recombinant hDAGL-β. *(A)* Representative gel of the dose response of LEI105 against DAGL-β. *(B)* Dose-response curve of recombinantly expressed DAGL-β inhibition by LEI105. LEI105 inhibited hDAGL-β with a pIC50 of 7.4 ± 0.07 (n=3).

The activity of LEI105 on human DAGL-β was confirmed using a biochemical assay with *para*-nitrophenylbutyrate as a surrogate substrate (pIC_{50} of 8.1 ± 0.07, n=4; Figure 3).

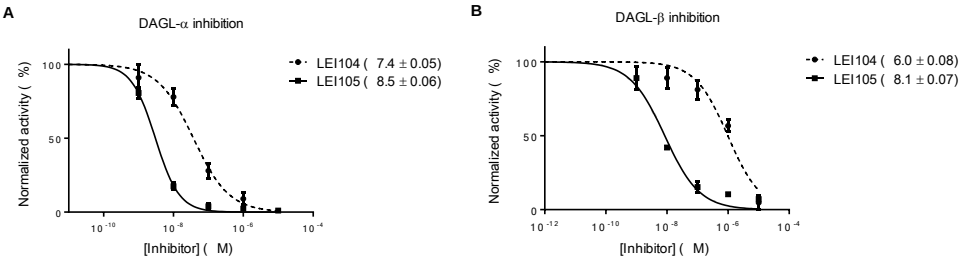

Figure 3. Dose-response curves of LEI104 and LEI105 against hDAGL-α and hDAGL-β as determined with a colorimetric assay based on the hydrolysis of PNP butyrate *(A).* Dose-response of LEI104 (pIC_{50} 7.4 ± 0.05; N=2, n=2) and LEI105 (pIC_{50} of 8.5 ± 0.06; N=2, n=2) against hDAGL-α. *(B)* Dose-response of LEI104 (pIC_{50} 8.1 ± 0.07; N=2, n=2) and LEI105 (pIC_{50} of 6.0 ± 0.08; N=2, n=2) against hDAGL-β.

Next, ABP MB064 was used to profile endogenous DAGL-β activity in twelve tissues from wild-type and DAGL-β knock-out mice. Spleen tissue was found to display the highest DAGL-β activity (Figure 4). This activity could be inhibited by LEI105 (Figure 1G).

Reduction of the α–keto group of LEI105 to the corresponding alcohol (compound **7**, scheme 1) led to a ~150 fold drop of activity against DAGL-α, thereby indicating that the α–carbonyl in LEI105 reacts with the active site serine hydroxyl to form a covalent, though reversible, enzyme-inhibitor hemiketal adduct. To determine the mode of action (reversible versus irreversible) of LEI105, an experiment in which human DAGL-α membranes were pre-incubated at the IC_{80} concentration of LEI105 or the irreversible DAGL inhibitor KT109 was performed (Figure 5).[15] The protein was separated from small molecule inhibitors via size exclusion column chromatography and remaining enzyme activity was visualized with MB064. No recovery of DAGL-α activity was found for KT109, whereas MB064 labeled DAGL-α exposed to LEI105 with similar intensity compared to DMSO treated DAGL-α (Figure 5). This indicates that LEI105 is a reversible inhibitor of DAGL-α.

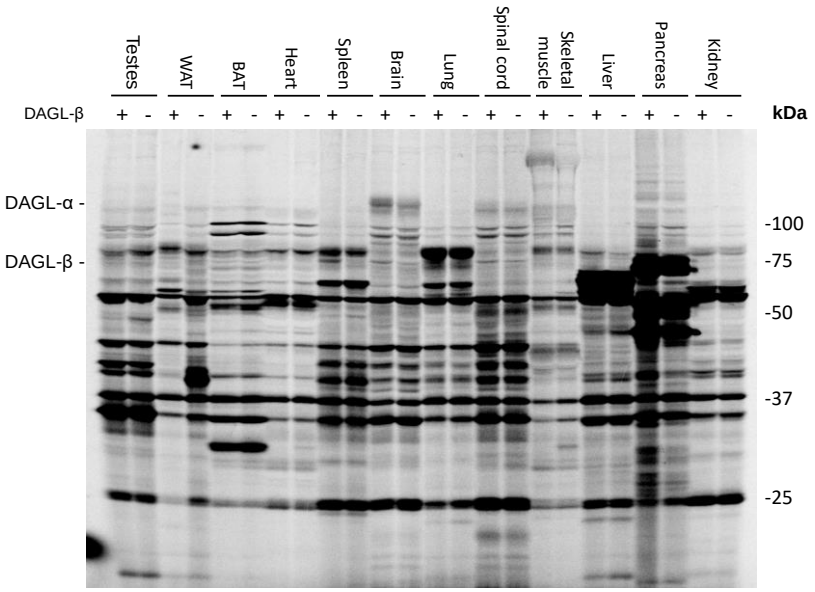

Figure 4. Screen of DAGL-β WT and KO tissues. DAGL-β WT and KO tissues were screened to obtain a tissue wide overview of DAGL-β activity. Mouse membrane proteome was incubated with 1 μM MB064 for min 30 at rt. A band at the molecular weight (~70 kD) of DAGL-β was present in the WT spleen tissue but absent in its KO counterpart. This indicates that MB064 can visualize DAGL-β activity in the spleen membrane proteome. (Abbreviations WAT: white adipose tissue; BAT: brown adipose tissue; (+) WT tissue and (−) DAGL-β KO tissue).

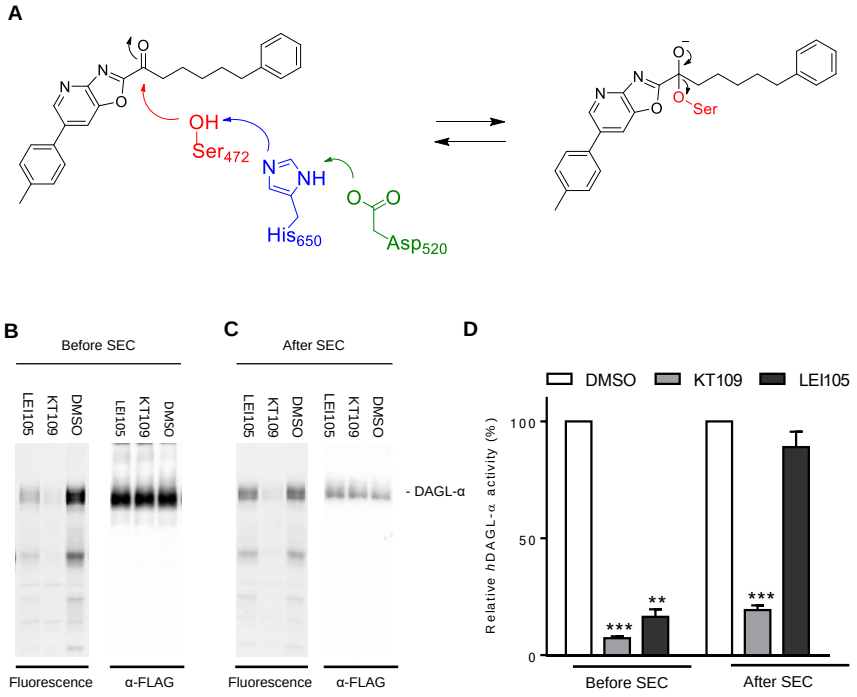

Figure 5. Reversibility assay against human recombinant DAGL-α. *(A)* Proposed mechanism of covalent reversible inhibition of DAGL-α by LEI105. *(B)* Fluorescence gel of DAGL-α labeling after treatment with KT109 and LEI105 before size exclusion chromatography (SEC) and anti-FLAG western blot of the same gel to control for protein loading. *(C)* Fluorescence gel of DAGL-α labeling after SEC of the same protein samples. DAGL-α labeling is regained after LEI105 treatment but still absent after treatment. (*D*) Schematic representation of the size exclusion chromatography (SEC) experiment that shows reversibility of LEI105 in recombinant DAGL-α (n = 3, full fluorescent gel and western blot are given in the supporting information). Statistical analysis: 2-way ANOVA (*** = $p < 0.001$; ** = $p < 0.01$ vs vehicle).

Determining proteome-wide selectivity of LEI105 using comparative and competitive chemoproteomics

To investigate the selectivity of LEI105 in the mouse brain proteome, comparative and competitive ABPP with a broad-spectrum FP-based probe (TAMRA-FP) and the DAGL-α targeting ABP, MB064 was used. As a reference, the widely used β-lactone-based DAGL-inhibitors THL and OMDM-188, two highly potent non-selective covalent and irreversible serine hydrolase inhibitors were used.[8,14] In our experimental setup, both compounds blocked labeling of at least 4 serine hydrolases at concentrations as low as 1 μM, including ABHD6 and ABHD12, enzymes involved in 2-AG metabolism in the brain (Figure 6 A,B).

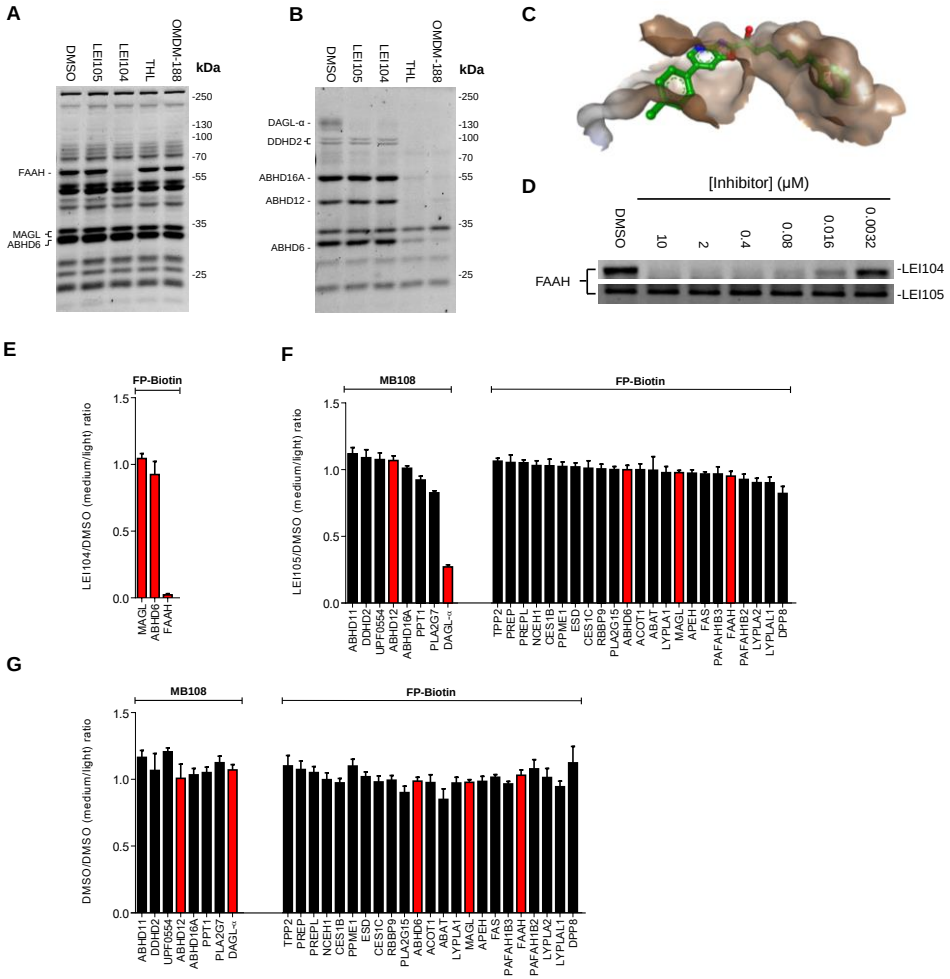

Figure 6. Selectivity of LEI105. *(A)* Competitive ABPP in the mouse brain membrane proteome with LEI104 (10 µM), LEI105 (10 µM), OMDM188 (1 µM) and THL (1 µM) using TAMRA-FP (500 nM). *(B)* Same experiment as in (a) with THL based ABP MB064 (250 nM) showing excellent selectivity of LEI105 at 10 µM compared to THL and OMDM188. *(C)* One possible LEI105-like conformer in a previously reported co-crystal structure of FAAH, showing a steric clash between the toluyl group and FAAH. *(D)* Activity of LEI104 and LEI105 against FAAH in a concentration response experiment in the mouse brain membrane proteome using TAMRA-FP (500 nM, full gels are given in the supporting information). *(E)* Chemoproteomic competition between LEI104 (10 µM) and FP-biotin (5 µm) for FAAH, MAGL and ABHD6, showing that the chemoproteomic settings using FP-biotin are compatible with reversible α-ketoheterocycles. *(F)* MB108 and FP-biotin based chemoproteomic analysis of serine hydrolase activities in the mouse brain membrane proteome treated with LEI105 (10 µM). DAGL-α labeling is reduced to over 70%. *(G)* Chemoproteomic control experiment shows equal isotopic labeling and detection of peptides from MB108 and FP-biotin labeled serine hydrolases. Enzymes known to be directly involved in endocannabinoid biosynthesis and metabolism are highlighted in red. (n = 3-4 independent chemoproteomics experiments; Error bars represent ± s.e.m. of medium over light ratios of quantified peptides (minimum of two unique peptides per enzyme). Only unique proteins are given for MB108, all detected proteins including proteins

overlapping between the probes are given in the supporting information. See supplementary data set **1** for complete proteomic data.

In previous studies, fatty acid amide hydrolase (FAAH) was identified as a major off-target for LEI104. In stark contrast to LEI104, which inhibited FAAH labeling with a pIC_{50} of 7.8 ± 0.04 (n=3) (Figure 6A, 7), LEI105 did not block FAAH labeling up to a concentration of 10 µM (n=3) (Figure 6A, D). Of note, LEI105 did not inhibit labeling of any other band either, it can be concluded that LEI105 is highly selective at least within the panel of serine hydrolases labeled by TAMRA-FP and MB064. To explain this remarkable selectivity of LEI105 for DAGLα/β over FAAH, a detailed investigation using a co-crystal structure of FAAH with OL-135 (pdb: 2WJ1 and 2WJ2) was performed.[26] *In silico* modification of the heterocyclic part of OL-135, in the presence of the protein receptor, to a LEI105 like conformer revealed a steric clash of the toluoyl moiety of LEI105 with the substrate channel of FAAH, thereby possibly explaining the high selectivity of LEI105 over FAAH compared to its analog LEI104 (Figure 6C).

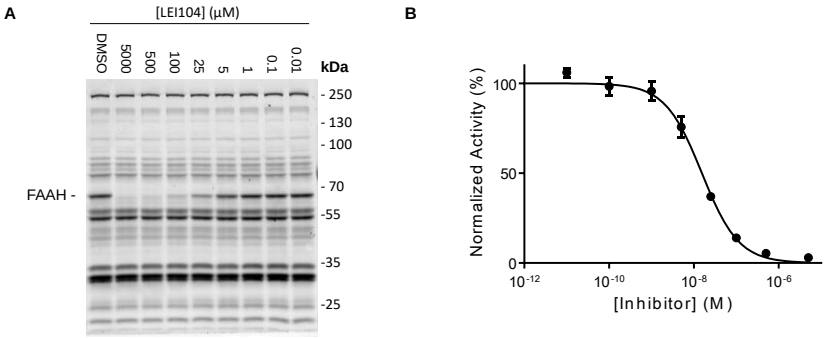

Figure 7. Activity of LEI104 against FAAH. *(A)*. Dose-response of LEI104 against FAAH in the mouse brain membrane proteome as determined by competitive ABPP using ABP TAMRA-FP (500 nM for 20 min at rt). *(B).* Dose-response curve of gel based FAAH inhibition assay pIC_{50} 7.8 ± 0.04 (n = 3).

Considering that the human serine hydrolase family contains approximately 200 family members,[27] the selectivity of LEI105 in the brain proteome was examined in a broader and more detailed manner. To this end, a semi-quantitative chemoproteomics protocol was adapted. This protocol was previously applied to determine the selectivity profile of the irreversible inhibitor KT-109. MB108 and FP-Biotin, a biotinylated version of MB064 and TAMRA-FP respectively, were used for this method. This methodology allows for a more accurate quantification avoiding band overlap (as observed with gel-based assays) and enables screening over a broader range of specified serine hydrolases. First, equal isotopic labeling and detection of light and medium peptides from proteins targeted by both ABPs was validated (Figure 6G). Next, the selectivity of LEI105 in this chemoproteomic assay was investigated. LEI105 (10 µM, 30 min) did not reduce labeling of the detected serine

hydrolases by more than 20%, except for DAGL-α (Figure 6F). In addition, LEI105 was tested in biochemical assays using recombinant human ABHD6 and MAGL and in a cannabinoid CB_1 receptor radioligand displacement assay. No significant interaction (pK_i < 5) with these proteins of the endocannabinoid system was found (Figure 8). Together these results indicate that LEI105 is a highly selective DAGL inhibitor.

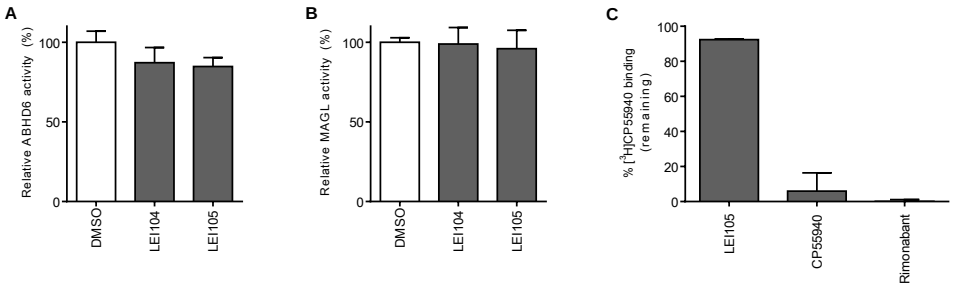

Figure 8. Selectivity of LEI105. *(A).* Relative MAGL activity in the presence of 10 μM LEI104 or LEI105 as determined with the glycerol-based natural substrate assay. *(B).* Relative ABHD6 activity in the presence of 10 μM LEI104 or LEI105 as determined with the glycerol-based natural substrate assay *(C)* Radioligand displacement assay for the CB1 receptor. LEI105 (10 μM) shows no affinity for the CB1 receptor.

LEI105 reduces 2-AG levels in Neuro2A cells

To test the cellular activity of LEI105, Neuro2A cells were used. Neuro2A is a mouse neuroblastoma cell line known to express both DAGL-α and DAGL-β.[28] First, the presence of the mRNA transcripts of both DAGLs was confirmed. Interestingly, it was found that DAGL-β mRNA levels are ~128-fold higher, compared to DAGL-α, as determined by qPCR. In line, DAGL-α protein activity was below the detection limit of our ABPP assay, whereas a fluorescent band at the expected molecular weight of DAGL-β was detected using MB064. The identity of the band at ~70 kD was confirmed by competition with three DAGL inhibitors with a different chemotype (THL, LEI105 and KT109), all 3 inhibitors blocked labeling of the band at ~70 kD, while the control inhibitor for KT109 (KT195, Supporting Figure 1) developed by Hsu *et al.*[15] did not block labeling of the band at ~70 kD. This confirmed the identity of the band as DAGL-β (Figure 9).

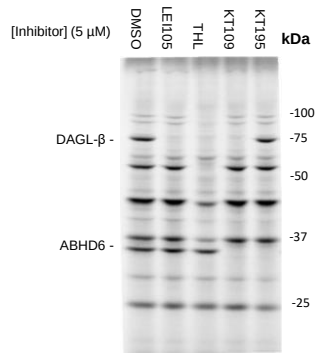

Figure 9. Validation of endogenous DAGL-β labeling by MB064 in Neuro2A cells. Labeling of Neuro2A membrane fractions by MB064 (2 µM, 20 min at rt) showed a fluorescent band at ~70 kDa corresponding to the molecular weight of DAGL-β. This signal was inhibited by DAGL inhibitors THL, LEI105 and KT109. The signal at ~70 kDa was not inhibited by the reported control probe for KT109.[5] These data together indicate that the fluorescent band at ~70 kDa corresponds with the enzyme DAGL-β. No fluorescent band was observed at ~120 kDa, the molecular weight of DAGL-α.

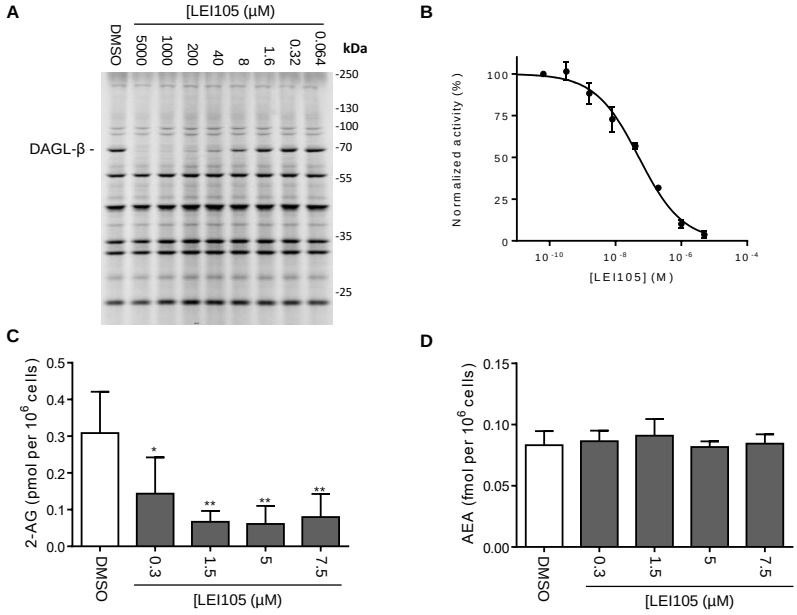

Figure 10. Cellular activity of LEI105. *(A)* Representative gel of concentration dependent inhibition of endogenous DAGL-β in vitro in the Neuro2A proteome as determined with ABP MB064. *(B)* Dose response curve of DAGL-β inhibition as determined with competitive ABP MB064 (± SEM, n = 3). *(C) In situ* treatment of Neuro2A cells (1h, 37 °C) dose dependently decreased basal 2-AG levels while keeping anandamide (AEA) levels *(D)* constant (mean ± SEM; n =4). Statistical analysis: 2-way ANOVA (*** = $p < 0.001$; ** = $p < 0.01$; * = $p < 0.05$ vs vehicle).

LEI105 selectively reduced DAGL-β labeling in a concentration dependent manner with a pIC_{50} of 7.3 ± 0.07 (Figure 10A, B). Of note, no inhibition of ABHD6 was observed. Next, in a targeted lipidomics experiment the effect of LEI105 on the cellular levels of 2-AG and anandamide was determined. A concentration-dependent reduction of 2-AG was found in Neuro2A cells, whereas anandamide levels were unaffected (Figure 10C, D). To test the activity of LEI105 in a human cell line, the PC3 cell line was used. DAGLβ activity in PC3 cells was confirmed in the same manner as in Neuro2A cells. All 3 DAGL inhibitors (THL, LEI105 and KT109) blocked MB064 labeling of a band at ~70 kD, while KT195 did not, confirming that the band at ~70kD is DAGL-β (Figure 11). LEI105 reduced 2-AG levels, but no change in *sn*-1-stearoyl-2-arachidonoyl-glycerol substrate levels of DAGL was detected, which may suggest that DAG species are rapidly converted into other membrane constituents, such as phosphatidic acid by DAG-kinases. Interestingly, arachidonic acid levels were reduced by LEI105 treatment of PC3 cells (Figure 11C). This may indicate that downstream metabolic pathways of 2-AG signaling are also affected and that the biosynthesis of 2-AG is the rate-limiting step. This is in line with a previously reported reduction of arachidonic acid levels in DAGL-α knockout mice and after inhibition with KT109 in mouse liver.[15, 5]

LEI105 reduces synaptic transmission in hippocampus

To demonstrate a physiological effect of the inhibition of 2-AG biosynthesis by LEI105, the attention was focused on hippocampal slice preparations in which depolarization-induced suppression of inhibition (DSI) is thought to be mediated via 2-AG-induced activation of presynaptic cannabinoid CB_1 receptors.[29,30] Experimental evidence, which supports a role of DAGL-α in DSI, has been obtained through the use of genetically engineered mice that constitutively lack DAGL-α. DSI was absent in these DAGL-α knock-out mice, but not in their DAGL-β knock-out counterparts.[5,10] Of note, anandamide levels were also reduced in these DAGL-α knock-out mice. Acute DAGL inhibition studies with chemical tools would, therefore, provide an additional line of evidence to verify the role of DAGL-α in DSI. Pharmacological intervention studies with the two highly potent non-selective DAGL inhibitors, THL and OMDM-188, however, have challenged the unequivocal role of the DAGLs in DSI. Multiple groups reported a suppression of DSI by THL and/or OMDM-188,[31-36] whereas other groups did not find any inhibitory effect of THL and/or OMDM-188.[37,38] The discrepancy between the genetic model and the pharmacological studies, led to the alternative hypothesis that 2-AG is released from pre-formed lipid stores instead of the ‘on demand’ production of 2-AG.[39,40]

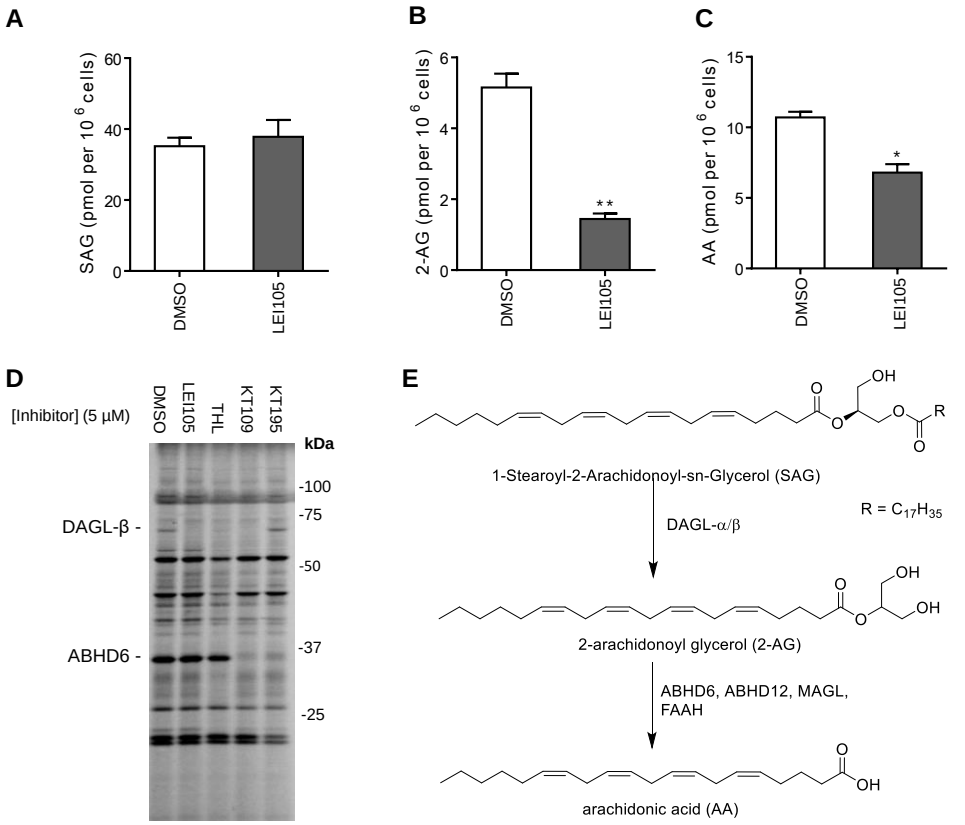

Figure 11. Cellular activity of LEI105 in PC3 cells. *(A)* In situ treatment of PC3 cells with LEI105 (7.5 µM for 4h; 37 ºC) did not affect SAG levels but decreased basal 2-AG *(B)* and AA *(C)* levels. *(D)* Labeling of PC3 membrane fractions by MB064 (2 µM, 20 min at rt) showed a fluorescent band at ~70 kDa, the molecular weight of DAGL-β. This signal could be inhibited by DAGL inhibitors THL, LEI105 and KT109. The signal at ~70 kDa was not inhibited by the reported control probe for KT109.[5] These data together indicate that the fluorescent band at ~70 kDa corresponds with the enzyme DAGL-β, and that DAGL-β is expressed and active in the PC3 cell line. No fluorescent band was observed at ~120 kDa, the molecular weight of DAGL-α. *(E)* Schematic representation of the current model of 2-AG biosynthesis and degradation. Statistical analysis: 2-way ANOVA (*** = $p < 0.001$; ** = $p < 0.01$; * = $p < 0.05$ vs vehicle).

Here, cannabinoid CB_1 receptor-dependent DSI in CA1 pyramidal neurons in hippocampal slices with the selective DAGL inhibitor was investigated. Pre-incubation and continuous application of 10 µM LEI105 had no effect on the amplitude of the stimulus-evoked inhibitory post-synaptic currents (IPSC) (271 ± 22 pA) compared to control (276 ± 32 pA). In control conditions, a DSI response could be evoked which decayed back with an exponential time course (τ = 34 sec) to baseline levels. DSI was quantified as the reduction in IPSC amplitude averaged over the first 15 sec after its induction. DSI evoked in slices treated with LEI105 was smaller than DSI induced in control slices (18 ± 7%, n=15 and

36 ± 4%, n=18, respectively; $p<0.05$, Student's t-test) (Figure 12). However, it is clear that DSI is not completely blocked in the presence of LEI105, which suggests that in addition to on demand 2-AG synthesis, the recruitment of 2-AG pools may contribute to DSI.[40] Alternatively, other endocannabinoids (e.g. anandamide) may be involved. Of note, at 10 μM LEI105 was still selective in our experimental set up and did not displace ^{3}H-CP55940 from the CB_1 receptor (Figure 8), a result that excludes direct antagonism of the CB_1 receptor by LEI105. Thus, the data support the hypothesis of a major, but not exclusive, role of 'on demand' production of 2-AG, which is responsible for the cannabinoid CB_1 receptor-mediated synaptic plasticity.[33]

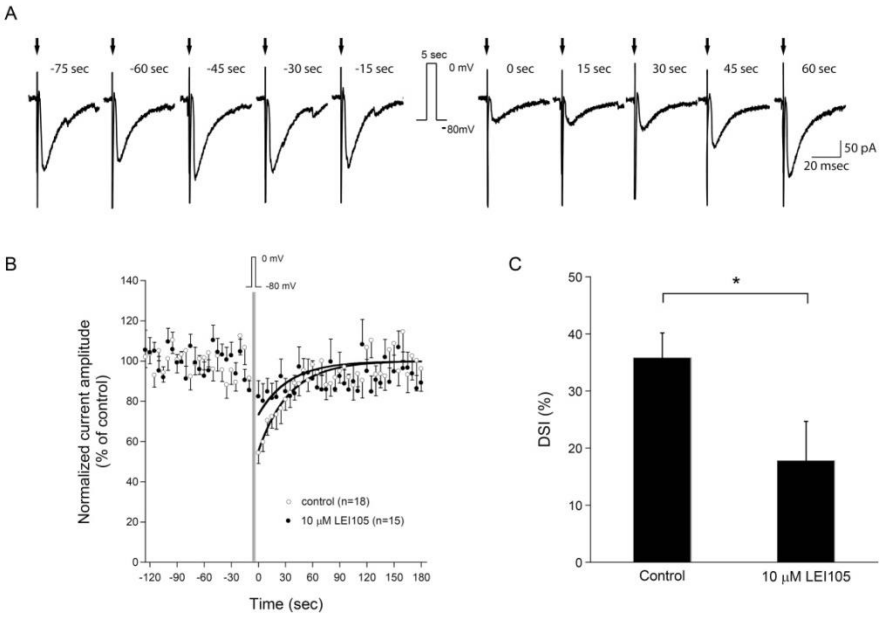

Figure 12. DSI is reduced in hippocampal slices treated with 10 μM LEI015. *(A)* Example of a typical whole-cell voltage-clamp recording of evoked inhibitory post-synaptic currents (IPSCs) in a CA1 pyramidal neuron under control conditions. IPSCs are evoked every 5 seconds, but for clarity, IPSCs shown here are representative traces recorded every 15 seconds. DSI is induced with a 5-sec duration depolarization from -80 mV to 0 mV and is observed as a marked and brief reduction of IPSC amplitude following the depolarization. *(B)* Averaged IPSC amplitude recorded every 5 seconds in CA1 neurons from vehicle-treated slices (DMSO) and from slices pre-incubated at least 30 minutes and in the continuous presence of LEI 105 (10 μM). The dark lines represent the single exponential fit of the recovery phase following the depolarizing step. *(C)* Initial DSI amplitude under control conditions (DMSO) and in the presence of LEI105 (10 μM). (* $p < 0.05$ vs vehicle)

Conclusions

In conclusion, comparative and competitive chemproteomics using a DAGL-α targeting ABP (MB064) in combination with the broad-spectrum probe (TAMRA-FP) was applied to identify and characterize the reversible DAGL inhibitor LEI105. This inhibitor was found to be an excellent tool to study the enzymatic role of DAGL-α in a neuronal setting and provides a critical counterpart to currently available DAGL knock-out mice. This was exemplified in Neuro2A cells (where LEI105 reduced 2-AG levels, but not AEA levels) and in intact hippocampal brain slices (where a clear suppression of DSI was observed in the presence of LEI105). Using this combination of activity-based probes in a chemoproteomic setting many lipases involved in the regulation of endocannabinoid levels (e.g. DAGL-α, ABHD6, ABHD12, MAGL and FAAH) in the brain are targeted with high affinity. This opens the door to broadly apply this methodology to identify and characterize not only covalent irreversible inhibitors, but also reversible inhibitors that target DAGL and other enzymes involved in 2-AG biosynthesis and metabolism. Identification of reversible inhibitors is important, because covalent irreversible inhibitors can potentially lead to toxicity and immunogenicity of covalent inhibitor-protein complexes and selectivity issues using reactive covalent warheads. Reversible inhibitors have the additional intrinsic advantage to enable a better control of partial inhibition of their target enzyme. This is especially important with respect to endocannabinoid signaling in the CNS, since complete blockade of cannabinoid CB_1 receptor signaling in the CNS may lead to severe side effects.[41] Thus, this feature can play an important factor in the development of clinical candidates to provide therapeutic solutions for diseases, such as obesity, related metabolic disorders and neuroinflammation, in which excessive 2-AG signaling or its metabolites play an important factor.

Experimental Methods

Synthetic procedures

General remarks

All reactions were performed using oven or flame-dried glassware and dry solvents. Reagents were purchased from Sigma Aldrich, Acros and Merck and used without further purification unless noted otherwise. All moisture sensitive reactions were performed under an argon atmosphere. Traces of water were removed from starting compounds by co-evaporation with toluene.

^{1}H- and ^{13}C-NMR spectra were recorded on a Bruker AV 400 MHz spectrometer at 400.2 (^{1}H) and 100.6 (^{13}C) MHz or a Bruker DMX-600 spectrometer 600 (^{1}H) and 150 (^{13}C) MHz using $CDCl_3$ or CD_3OD as solvent, unless stated otherwise. Chemical shift values are reported in ppm with tetramethylsilane or solvent resonance as the internal standard ($CDCl_3$ δ 7.26 for ^{1}H, δ 77.0 for ^{13}C, CD_3OD: δ 3.31 for ^{1}H). Data are reported as follows: chemical shifts (δ), multiplicity (s = singlet, d = doublet, dd = double doublet, td = triple doublet, t = triplet, q = quartet, quinted = quint, br = broad, m = multiplet), coupling constants *J* (Hz), and integration. HPLC purification was performed on a preparative LC-MS system (Agilent 1200 serie) with an Agilent 6130 Quadruple MS detector. High-resolution mass spectra (HRMS) were recorded on a Thermo Scientific LTQ Orbitrap XL. Flash chromatography was performed using SiliCycle silica gel type SiliaFlash P60 (230 – 400 mesh). TLC analysis was performed on Merck silica gel 60/Kieselguhr F254, 0.25 mm. Compounds were visualized using either Seebach's reagent (a mixture of phosphomolybdic acid (25 g), cerium (IV) sulfate (7.5 g), H_2O (500 mL) and H_2SO_4 (25 mL)) or a $KMnO_4$ stain (K_2CO_3 (40 g), $KMnO_4$ (6 g), H_2O (600 mL) and 10% NaOH (5 mL)).

3-(benzyloxy)pyridin-2-amine (2): Benzylbromide (2.2 mL, 18.2 mmol) was dissolved in DMF (90 mL), 2-hydroxy-3-aminopyridine (2.0 g, 18.2 mmol) and Cs_2CO_3 (6.4 g, 18.2 mmol) were added and the reaction mixture was stirred over weekend. The reaction mixture was diluted with EtOAc/H_2O (1:1, 100 mL), the layers were separated and the water layer was extracted with EtOAc. The combined organic layers were washed with H_2O and brine before they were dried on $MgSO_4$, filtered and concentrated under reduced pressure. The residue was purified by flash chromatography over silica gel using pentane/ethyl acetate (20:80) with 1% Et_3N. This yielded **2** (2.0 g, 10.2 mmol, 56%) as a pale yellow solid. ^{1}H NMR (400 MHz, $CDCl_3$) δ 7.67 (d, *J* = 5.1 Hz, 1H), 7.46 – 7.31 (m, 5H), 6.96 (d, *J* = 7.8 Hz, 1H), 6.59 (dd, *J* = 7.8, 5.1 Hz, 1H), 5.06 (s, 2H), 4.73 (s, 2H). ^{13}C NMR (101 MHz, $CDCl_3$) δ 150.33, 141.58, 139.10, 136.36, 128.78 (2C), 128.38, 127.67 (2C), 116.90, 113.69, 70.28. IR: 3468.6, 3290.3, 3130.7, 1626.5, 1485.7, 1452.2, 1205.9, 738.3, 697.

3-(benzyloxy)-5-bromopyridin-2-amine (3): (2.0 g, 9.99 mmol) was dissolved in ACN and cooled to 0°C. N-bromosuccinimide (1.79 g, 10 mmol) was added in portions. The reaction mixture was stirred for 15 minutes before the solvent was removed under reduced pressure. The residue was taken up in EtOAc/H_2O (1:1) and the layers were separated. The organic layer was washed with saturated $NaHCO_3$ (aq.) and brine before it was dried on $MgSO_4$, filtered and concentrated under reduced pressure. This yielded **3** (2.2 g, 8.0 mmol, 80%).^{1}H NMR (400 MHz, $CDCl_3$) δ 7.73 (d, *J* = 1.9 Hz, 1H), 7.44 – 7.33 (m, 5H), 7.08 (d, *J* = 1.9 Hz, 1H), 5.04 (s, 2H), 4.77 (s, 2H). ^{13}C NMR (101 MHz, $CDCl_3$) δ 149.07, 141.86, 139.32, 135.59, 128.88 (2C), 128.67, 127.82(2C), 119.65, 106.95, 70.68. Spectroscopic data are in agreement with those reported. [9]

3-(benzyloxy)-5-(p-tolyl)pyridin-2-amine (4): 4-methylphenylboronic acid (120 mg, 0.88 mmol), **3** (200 mg, 0.72 mmol), Na_2CO_3 (228 mg, 2.16 mmol) and Pd(dppf)Cl_2 (5 mg, 0.006 mmol) were dissolved in 5 mL 1.2-dimethoxyethane/H_2O (20:1). The mixture was heated for 8h to 150 °C using microwave irradiation. The reaction mixture was diluted with EtOAc and washed with H_2O and brine. The organic layer was dried on $MgSO_4$, filtered and concentrated under reduced pressure. The residue was purified by flash chromatography using pentane/ethyl acetate (70:30) with 1% Et_3N. This yielded **4** (138 mg, 0.48mmol, 66%) as a brown solid. ^{1}H NMR (400 MHz, $CDCl_3$) δ 7.90 (d, *J* = 1.8 Hz, 1H), 7.48 – 7.34 (m, 8H), 7.22 – 7.19 (m, 2H), 5.14 (s, 2H), 4.84 (s, 2H), 2.38 (s, 3H). ^{13}C NMR (101 MHz, $CDCl_3$) δ 149.24, 141.68, 136.88, 136.48, 136.20, 135.66, 129.71 (2C), 128.86 (2C), 128.52, 127.82 (2C), 127.68, 126.44 (2C), 116.08, 70.52, 21.20.

2-amino-5-(p-tolyl)pyridin-3-ol (5): Compound **4** (170 mg, 0.59 mmol) was dissolved in MeOH. Pd/C (50 mg) was added and the mixture was stirred for 1h under a H_2 atmosphere. The reaction mixture was filtered over celite and concentrated under reduced pressure. The residue was purified by flash chromatography over silica gel using CH_2Cl_2/MeOH (90:10). This yielded **5** (77 mg, 0.38 mmol, 65%) as a green solid. ^{1}H NMR (400 MHz, MeOD) δ 7.61 (d, *J* = 1.9 Hz, 1H), 7.37 (d, *J* = 8.1 Hz, 2H), 7.20 (d, *J* = 7.9 Hz, 2H), 7.16 (d, *J* = 2.0 Hz, 1H), 2.34 (s, 3H). ^{13}C NMR (101 MHz, MeOD) δ 150.69, 142.66, 137.81, 136.50, 133.21, 130.54 (2C), 128.77, 126.98 (2C), 119.09, 21.08. IR: 3339.8, 2974.3, 2886.6, 1648.4, 1380.7, 1087.5, 1045.3, 879.6, 615.3.

Ethyl 2-hydroxy-7-phenylheptanimidate (6): Acetyl chloride (1 mL, 14 mmol) was added drop-wise to a mixture of EtOH/$CHCl_3$ (1:1) at 0 °C, and the solution was subsequently stirred for 30 min. 2-hydroxy-7-phenylheptanenitrile (213 mg, 1.05 mmol) dissolved in $CHCl_3$ (1.0 mL) was added drop-wise at 0°C. After the reaction mixture was stirred for 2h it was allowed to warm to rt and the solvents were removed at 25°C under reduced pressure. The obtained solid imidate (**6**) was directly used for the next reaction.

6-phenyl-1-(6-(p-tolyl)oxazolo[4,5-b]pyridin-2-yl)hexan-1-ol (7): Compound **5** (77 mg, 0.38 mmol) dissolved in EtOH (2 mL) was added to a sealed microwave tube. Pyridine (0.04 mL, 0.49 mmol) was added and the mixture was heated for 15 min to 80 ^{o}C using microwave irradiation. Imidate **6** (123 mg, 0.49 mmol) dissolved in EtOH (1.0 mL) was added and the mixture was heated to 80 ^{o}C for 6h using microwave irradiation. The reaction mixture was concentrated under reduced pressure and purified by flash chromatography over silica gel using CH_2Cl_2/MeOH (95:5). This yielded compound **7** (32 mg, 0.082 mmol; 17%) as a brown solid. ^{1}H NMR (400 MHz, MeOD) δ 8.69 (d, *J* = 1.8 Hz, 1H), 8.20 (d, *J* = 1.9 Hz, 1H), 7.55 (d, *J* = 7.9 Hz, 2H), 7.29 (d, *J* = 7.8 Hz, 2H), 7.23 – 7.17 (m, 2H), 7.13 – 7.08 (m, 3H), 4.96 – 4.90 (m, 1H), 2.57 (t, *J* = 7.7 Hz, 2H), 2.37 (s, 3H), 1.98 (p, 2H), 1.66 – 1.53 (m, 2H), 1.48 – 1.35 (m, 2H). ^{13}C NMR (101 MHz, MeOD) δ 173.16, 154.99, 145.94, 145.00, 143.77, 139.61, 136.36, 135.57, 130.97 (2C), 129.38 (2C), 129.24 (2C), 128.44 (2C), 126.63, 118.55, 68.80, 36.76, 36.14, 32.60, 29.91, 26.05, 21.17. IR: 3351.4 (br), 3030.3, 2923.0, 2859.6, 1478.6, 1378.5, 1265.5, 1103.1, 813.3, 740.2, 694.8. HRMS (ESI+) m/z: calculated for $C_{25}H_{26}N_2O_2$ (M + H^+) 387.2067; found 387.2072.

6-phenyl-1-(6-(p-tolyl)oxazolo[4,5-b]pyridin-2-yl)hexan-1-one(8, LEI105): To a solution of **7** (21 mg, 0.05 mmol) in CH_2Cl_2 (2 mL) was added Dess-Martin periodinane (35 mg, 0.075 mmol) and the reaction mixture was stirred under argon atmosphere overnight. The reaction mixture was quenched with saturated $NaHCO_3$ (aq). The layers were separated and the organic layer was extracted with CH_2Cl_2. The combined organic layers were washed with brine, dried on $MgSO_4$, filtered and concentrated under reduced pressure. The residue was purified by flash chromatography over silica gel using toluene/ethyl acetate (90:10) with 1% Et_3N. This yielded compound **8** (LEI105) (14 mg, 0.036 mmol, 73%) as a white solid.^{1}H NMR (400 MHz, $CDCl_3$) δ 8.97 (d, *J* = 2.0 Hz, 1H), 8.09 (d, *J* = 2.0 Hz, 1H), 7.54 (d, *J* = 8.1 Hz, 2H), 7.34 (d, *J* = 8.0 Hz, 2H), 7.31 – 7.22 (m, 2H), 7.22 – 7.13 (m, 3H), 3.29 (t, *J* = 7.4 Hz, 2H), 2.64 (d, *J* = 8.0 Hz, 2H), 2.44 (s, 3H), 1.93 – 1.81 (m, 2H), 1.71 (dt, *J* = 15.4, 7.6 Hz, 2H), 1.55 – 1.44 (m, 2H). ^{13}C NMR (101 MHz, $CDCl_3$) δ 190.20, 158.58, 152.99, 148.15, 144.05, 142.37, 138.98, 137.48, 133.95, 130.09 (2C), 128.37 (2C), 128.26 (2C), 127.49 (2C), 125.67, 117.68, 39.69, 35.69, 31.15, 28.69, 23.71, 21.20. IR: 3029.9, 2921.6, 2857.0, 1705.9, 1529.6, 1371.5, 1232.4, 1000.0, 819.7, 749.7, 697.2. HRMS (ESI+) m/z: calculated for $C_{25}H_{24}N_2O_2$ (M + H^+) 385.1911; found 385.1914. LCMS purity > 95%, retention time: 7.23, method: CH_3CN/H_2O 50-90%.

Biochemical methods

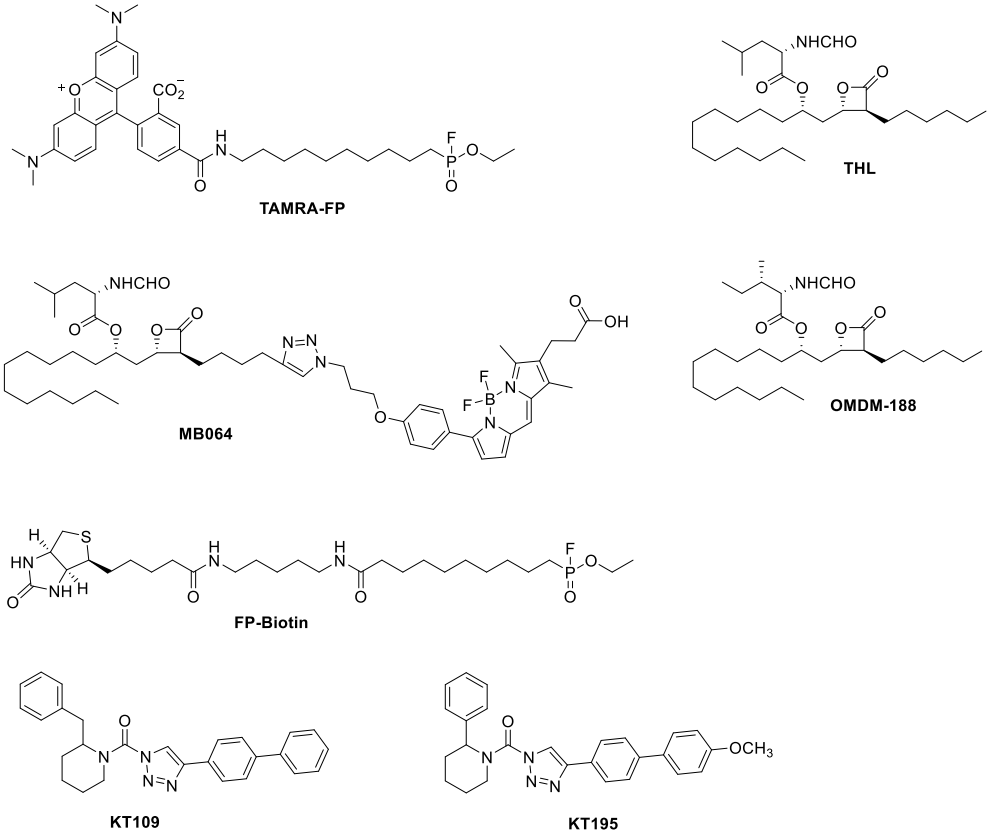

Additional Figure 1. Structures of inhibitors and probes used throughout the chapter. TAMRA-FP (Thermo fisher scientific), MB064[1], FP-Biotin (Santa Cruz Biotechnology), THL (Sigma Aldrich), OMDM-188[8], KT109 and KT195[15].

hDAGL-α/β plasmids. Full length human cDNA was purchased (Biosource) and cloned into mammalian expression vector pcDNA3.1, containing genes for ampicillin and neomycin resistance. hDAGL-α constructs were obtained as reported previously.[13] For proteins containing a FLAG-tag, a FLAG-linker was made from primers and cloned into the vector at the C-terminus of hDAGL-α or hDAGL-β. Two step PCR mutagenesis was performed to substitute the active site serine for an alanine in the hDAGL-β-FLAG, to obtain hDAGL-β-S443A-FLAG. All plasmids were grown in XL-10 Z-competent cells and prepped (Maxi Prep, Qiagen). Sequence analysis for the confirmation of the sequences was performed at the Leiden Genome Technology Centre.

Cell culture and membrane preparation. Cell culture and membrane preparation were performed as previously described.[13] In brief, HEK293T cells were grown in DMEM with

stable glutamine and phenolred (PAA), 10% New Born Calf serum, penicillin and streptomycin. Cell passage was performed every 2-3 days by resuspension in medium and seeding them to appropriate confluence. Membranes were prepared from transiently transfected HEK293T cells. 24h prior to transfection 10^7 cells were seeded in a 15 cm petri dish. A 3:1 mixture of polyethyleneimine (60µg) and plasmid DNA (20µg) in 2 mL serum free medium was added. The medium was refreshed after 24 hours, and after 72h the cells were harvested in 20 mL medium. Cells were isolated by centrifugation for 10 min at 1000 rpm and subsequent aspiration of the medium. The cell pellet was flash frozen in liquid nitrogen and stored at -80 ^{o}C until use.

Cell pellets were slowly thawed on ice and suspended in lysis buffer (20 mM HEPES pH 7.2, 2 mM DTT, 0.25 M sucrose, 1 mM $MgCl_2$, 1x protease inhibitor cocktail (Roche c*O*mplete EDTA free), 25 U/mL Benzonase). Three pulses with a polytrone (3 × 7 sec) were used to homogenize the suspension. After homogenization, the suspension was allowed to incubate for 10 min on ice. Ultracentrifugation (100.000 × g, 30 min, 4 ^{o}C, Beckman Coulter, Type Ti70 rotor) was used to separate the cytosolic fraction and the membrane fraction. The pellet (membrane fraction) was resuspended in storage buffer (20 mM HEPES pH 7.2, 2 mM DTT, 1x protease inhibitor cocktail (Roche c*O*mplete EDTA free)). The total protein concentration was determined with Quick Start Bradford assay (Biorad) or Qubit^{TM} protein assay (Invitrogen). The protein concentration was adjusted to 1 mg/mL before it was flash frozen in liquid nitrogen and stored at -80 ^{o}C until use.

Biochemical DAGL activity assay. The biochemical hDAGL-α assay was performed as reported previously.[13] In brief, the biochemical hDAGL-α activity assay is based on the hydrolysis of para-nitrophenylbutyrate (PNP-butyrate) by membrane preparations from HEK293T cells transiently transfected with hDAGL-α. Reactions were performed in 50 mM HEPES pH 7.2 buffer with 0.05 µg/µL (final protein concentration) hDAGL-α transfected membrane fractions. The colorimetric assay for DAGL-β activity was performed using the same methodology as for the DAGL-α assay, but hDAGL-β transfected HEK293T cell membranes were used.

Radioligand displacement assay. [^{3}H]CP55940 (specific activity 141.2 Ci/mmol) and GF-C filters were purchased from Perkin Elmer (Waltham, MA). Bicinchoninic acid (BCA) and BCA protein assay reagent were obtained from Pierce Chemical Company (Rochford, IL).The cell line stably expressing the hCB_1 receptor (CHOK1hCB1_bgal) was obtained from DiscoveRx.

Cell culture and membrane preparation for the radioligand displacement assay. CHOK1hCB_1_bgal cells were cultured in Ham's F12 Nutrient Mixture supplemented with 10% fetal calf serum, 1 mM glutamine, 50 µg/mL penicillin, 50 µg/ml streptomycin, 300 mg/mL hygromycin and 800 µg/mL geneticin in a humidified atmosphere at 37°C and 5%

CO_2. Cells were subcultured twice a week at a ratio of 1:20 on 10-cm ø plates by trypsinization. For membrane preparation the cells were subcultured 1:10 and transferred to large 15-cm diameter plates.

[^{3}H]CP55940 displacement assay. [^{3}H]CP55940 displacement assays to determine the cannabinoid CB1 binding affinity were performed as reported previously,[3] with the following changes: Membrane aliquots containing 5 µg (CHOK1hCB$_1$_bgal) of membrane protein in 100 µL assay buffer (50 mM Tris–HCl, 5 mM $MgCl_2$, 0.1% BSA, pH 7.4) were incubated at 30°C for 1 hr. Non-specific binding was determined in the presence of 10 µM AM630. Filtration was performed on GF/C filters, presoaked for 30 min with 0.25% PEI, using a Brandel harvester. Filter-bound radioactivity was determined in a β-counter.

Preparation of mouse tissue proteome. Mouse tissue were isolated according to guidelines approved by the ethical committee of Leiden University (DEC#13191). Mouse tissues were dounce homogenized in pH 7.2 lysis buffer A (20 mM HEPES pH 7.2, 2 mM DTT, 1 mM $MgCl_2$, 25 U/mL Benzonase) and incubated for 5 minutes on ice. The suspension was centrifuged (2500 × g, 3 min, 4 ^oC) to remove debris. The supernatant was collected and subjected to ultracentrifugation (100.000 × g, 45 min. 4 ^oC, Beckman Coulter, Type Ti70 rotor). This yielded the membrane fraction as a pellet and the cytosolic fraction in the supernatant. The membrane fraction was suspended in storage buffer (20 mM HEPES pH 7.2, 2 mM DTT). The total protein concentration was determined with Quick Start Bradford assay (Biorad) or Qubit^{TM} protein assay (Invitrogen). Membranes and supernatant were flash frozen in liquid nitrogen and stored in aliquots at -80 ^oC until use.

Activity based protein profiling on transiently transfected HEK293T cells. HEK293T cells were transfected with hDAGL-α-FLAG, hDAGL-β-FLAG or hDAGL-β-S443A-FLAG and the membranes were isolated following a protocol reported previously.[1] For DAGL-α ABPP assays, the membrane proteome (1 mg/mL, 20 µL) was incubated at rt with vehicle (DMSO) or inhibitor in 0.5 µL DMSO for 30 min. The sample was subsequently treated for 15 min with 250 nM (final concentration) ABP MB064 or 500 nM (final concentration) TAMRA-FP. The incubation protocols for DAGL-β constructs was similar except for the probe concentration and incubation time of MB064 (20 min, 2 µM final concentration). The reactions were quenched with 10 µL standard 3 × SDS PAGE sample buffer. The samples were directly loaded and resolved on SDS PAGE gel (10 % acrylamide). The gels were scanned using a ChemiDoc MP system (Cy3 settings, 605/50 filter) and analyzed using Image lab 4.1.

Activity based protein profiling in Neuro2A cells. Neuro2A cells were grown in DMEM with stable glutamine and phenolred, 10% New Born Calf serum, penicillin and streptomycin. Cells were passaged every 2-3 days by resuspension in medium and seeding

them to appropriate confluence. Before harvest, the Neuro2A cells were washed with serum free medium (3x). The cells were suspended in serum free medium and centrifuged at 1000 rpm for 10 min to pellet the cells. The cell pellets were flash frozen in liquid nitrogen and stored at -80 until lysis. The Neuro2A cells were suspended in lysis buffer (20 mM HEPES pH 7.2, 2 mM DTT, 1 mM $MgCl_2$, 25u/mL Benzonase) and dounce homogenized. The protein concentration was determined by Qubit™ protein assay (invitrogen) or Quick Start Bradford assay (Biorad) and samples were subsequently flash frozen and stored at -80 ^{o}C until use. Neuro2A proteome (2 mg/mL) was incubated with vehicle (DMSO) or inhibitor in 0.5 µL DMSO for 30 min at rt. The sample was subsequently treated with ABP MB064 (2 µM) for 20 min at rt before the reaction was quenched with standard 3 × SDS PAGE sample buffer. Gels were scanned using a ChemiDoc MP system (Cy3 settings, 605/50 filter) and analyzed using image lab 4.1. PC3 cells were maintained in F12K medium and subcultured and analyzed using the same protocol as for the Neuro2A cells.

Activity based protein profiling in mouse tissue. Tissue proteome (2 mg/mL) was incubated with vehicle (DMSO) or inhibitor in 0.5 µL DMSO for 30 min at rt and subsequently incubated for 15 min. with ABP MB064 (250 nM (final concentration) for DAGL-α detection or for 20 min. with 2 µM ABP MB064 (final concentration) for DAGL-β detection). The proteins were resolved and visualized using the same procedure as for the Neuro2A cells.

Western BLOT. Western blot procedure was performed as reported previously.[13] In brief, Proteins were transferred from gel to a PVDF membrane using a Trans-Blot® Turbo (BioRad). Enzymes containing a FLAG-tag were stained using rabbit anti-FLAG as primary antibody, and goat-anti-rabbit HRP as secondary antibody. The blot was developed in the dark using a 10 mL luminal solution, 100 µL ECL enhancer and 3 µL H_2O_2. Chemiluminescence was visualized using a ChemiDoc XRS (BioRad).

qPCR. For qPCR experiments, iTaq™ Universal SYBR® Green Supermix (BioRad) was used following the manufacturers protocol.

ABPP inhibitor activity measurements. The percentage of activity remaining was determined by measuring the integrated optical intensity of the fluorescent protein bands using Image lab 4.1. The relative intensity was compared to the vehicle treated proteins, which were set to 100%. IC50 and IC_{80} values were determined by plotting a log(inhibitor) vs. normalized response (variable slope) dose-response curve generated using Prism software (GraphPad).

Natural substrate based fluorescence assay. The natural substrate assay for DAGL-α, MAGL and ABHD6 activity were performed as reported previously.[25]

Size exclusion chromatography. Membrane fractions of DAGL-α-FLAG transfected HEK293T (1 mg/mL; 0.5 mL) cells were incubated with vehicle (DMSO), pIC_{80} concentration of LEI105 (6.5 ± 0.12) or the pIC_{80} concentration of KT109 (6.8 ± 0.19) for 30 minutes at rt. Small molecules were separated from proteins using 2 mL Zeba spin desalting columns (Thermo scientific) using the manufacturers protocol (3×). DAGL-α activity of the samples before and after size exclusion chromatography were analyzed using the ABPP method as described above. Western blot of the FLAG-tag signal was used to control for equal protein loading.

Lipid analysis PC3 cells. PC3 cells were cultured as described above. Before inhibitor treatment, the culture medium was removed and the cells were washed with warm (37 ^{o}C) serum-free medium (3x). The cells were treated with vehicle (DMSO) or inhibitor for 4h at 37 ^{o}C in serum-free medium. After 4h of incubation medium was removed and the cells were washed with cold (4^{o}C) DPBS (3x) and subsequently suspended in DPBS and pelleted. The cell pellet metabolome was extracted and analyzed as described previously.[5]

Lipid analysis Neuro2A cells. Neuro2A cells were cultured as described above. Before inhibitor treatment, the culture medium was removed and the cells were washed with warm (37 ^{o}C) serum free medium (3x). The cells were treated with vehicle (DMSO) or inhibitor for 1h at 37 ^{o}C in serum free medium. After 1h of incubation medium was removed and the cells were washed with cold (4^{o}C) PBS (3x) and subsequently suspended in PBS and pelleted. The PBS was removed and the cell pellet was flash frozen and stored at -80 ^{o} until endocannabinoid extraction.
Cell pellets were suspended in 100 µL 0.5% NaCl (aq.), and 510 µL 0.2% formic acid (vol/vol) in ACN containing internal standards (d_8-anandamide (6 pmol) and d_8-2-arachidonoyl glycerol (60 pmol)). The mixture was vortexed and loaded on a captiva ND lipid column (A5300635, Agilent technologies). Positive pressure was applied and the flow through was collected. The elution step was subsequently repeated with 500 µL and 250 µL 0.2% formic acid (vol/vol) in ACN/H_2O 95:5 (vol/vol). The combined elutes were concentrated in a speedvac and reconstituted in H_2O/MeOH 1:1 (vol/vol) for LC/MS analysis.

LC-Chip-MS/MS analysis. Endocannabinoids were measured using a chip-based nano liquid chromatography (LC) system coupled to a triple quadrupole mass spectrometer. The HPLC-Chip is inserted into the HPLC-Chip-MS interface, which mounts directly on the MS source. It includes a miniature camera for spray visualization, the loading mechanism for chip positioning, the microvalve for flow switching, and fluid connection ports for the nano-LC and microwell- plate autosampler.

Chromatographic conditions were achieved on a 1100 series LC-chip system (Agilent technologies, Walbron, Germany) consisting of a nanoflow pump, a capillary pump, a micro well plate auto sampler with thermostat and a LC-Chip/MS interface (chipcube). The chromatographic separations were performed on an ultra-high capacity chip including a 360 nL enrichment column and a 150 mm × 75 µm analytical column, both packed with a Polaris-HR-chip 3µm C18 phase (Agilent Technologies). The mobile phase was composed of 10mM formic acid/water (A) and ACN (B). The analytical gradient was performed in two steps: first, the 8ul sample was loaded on the enrichment column during an isocratic enrichment phase using the capillary pump delivering a mobile phase in isocratic mode composed of 40%B at a flow rate of 2 µL/min. The column was flushed with two wash cycles for 8min at 100%B to remove unretained components. Then, after the valve switches, a gradient starts at 45%B that linearly increases up to 80% B in 12min at a flow rate of 400nL/min. The column was then rinsed with 95%B for 2 minutes before returning to 45% B. The column was re-equilibrated for 5min prior to the next injection. The total analysis time was 20min for each run. During the analysis, the needle was washed with ACN/H_2O (1/1, v/v) commanded by an injection program.
A 6440 Triple quadrupole equipped with a nonoESI source operating in positive mode (Agilent technologies, Walborn, Germany) was used for MS detection. Capillary voltage was set to 1800V. The drying gas was set at a flow rate of 4 L/min and the source temperature was maintained at 365C. Quantification was obtained using static MRM (multiple reaction monitoring) mode of the transitions at m/z 379.3 → 287.2 for 2-AG, 348.3 → 62.2 for AEA and 387.3 → 294.2 for 2-AG-d8, 356.3 → 62.2 for AEA-d8 (internal standards). Mass hunter workstation (Agilent technologies) was used for instrument control. Raw MS data were processes using mass hunter quantitative analysis work station (Agilent technologies). AEA and 2AG was quantified by using an matrix matched internal standard calibration curve.

Proteomics

A schematic representation of the proteomic experiment is given in figure S2. Mouse brain proteome (500 µL, 2.0 mg/mL) membrane or soluble fraction was incubated with vehicle (DMSO) or inhibitor (10 µM) in DMSO for 30 minutes at rt. The proteome was labeled with MB108 (2.5 µM, 30 minutes, rt) or FP-Biotin (5 µM, 30 minutes, 37 ^{o}C). Subsequently the labeling reaction was quenched and excess probe was removed by chloroform methanol precipitation. Precipitated proteome was suspended in 500 µL 6M Urea/25 mM ammonium bicarbonate and allowed to incubate for 15 minutes. 5 µL (1 M DTT) was added and the mixture was heated to 65 ^{o}C for 15 minutes. The sample was allowed to cool to rt before 40 µL (0.5 M) iodoacetamide was added and the sample was alkylated for 30 minutes in the dark. 140 µL 10% (wt/vol) SDS was added and the proteome was heated for 5 minutes at 65 ^{o}C. The sample was diluted with 6 mL PBS. 100

µL of 50% slurry of Avidin−Agarose from egg white (Sigma-Aldrich) was washed with PBS and added to the proteome sample. The beads were incubated with the proteome > 2h. The beads were isolated by centrifugation and washed with 0.5% (wt/vol) SDS and PBS (3x). The proteins were digested overnight with sequencing grade trypsin (Promega) in 100 µL Pd buffer (100 mM Tris, 100 mM NaCl, 1 mM CaCl2, 2 % ACN and 500 ng trypin) at 37 ^{o}C with vigorous shaking. The pH was adjusted with formic acid to pH 3 and the beads were removed. The peptides were isotopically labeled by on stage tip dimethyl labeling.

On–stage tip dimethyl labeling (adapted from Li, Kuo *et al.* 2013[6]). The stage tips were made by inserting C_{18} material in a 200 µL pipet. The stepwise procedure given in the table below was followed for stage tip desalting and dimethyl labeling. The solutions were eluted by centrifugal force and the constitutions of the reagents are given below.

Step	Solution	Centrifugation speed
Conditioning	Methanol (50 µL)	2 min 600g
Conditioning	Stage tip solution B (50 µL)	2 min 600g
Conditioning	Stage tip solution A (50 µL)	2 min 600g
Loading	Load samples on stage tips	2.5 min 800g
Washing	Stage tip solution A (100 µL)	2.5 min 800g
Dimethyl labeling	Load 20 µL L or M reagents on stage tip (5X)	5 min 400g
Washing	Stage tip solution A (100 µL)	2.5 min 800g
Elution	Stage tip solution B (100 µL)	2.5 min 800g

Stage tip solution A: Stage tip solution A is 0.5% (vol/vol) FA in H_2O. (Freshly prepared solution)
Stage tip solution B: Stage tip solution B is 0.5% (vol/vol) FA in 80% (vol/vol) ACN/H_2O. (Freshly prepared solution).

Dimethyl labeling reagents

Light labeling reagent	Final concentration	Volume
Phosphate buffer (50 mM; pH 7.5)		900 µL
CH_2O (light)		50 µL
$NaBH_3CN$ (0.6 M)	0.03 M	50 µL

Medium labeling reagent	Final concentration	Volume
Phosphate buffer (50 mM; pH 7.5)		900 µL
CD_2O (Medium)		50 µL
$NaBH_3CN$ (0.6 M)	0.03 M	50 µL

After the final elution step, the desired heavy and light samples were combined and concentrated on a speedvac to remove the ACN. The residue was reconstituted in 95:3:0.1 H_2O/ACN/FA (vol/vol) before LC/MS analysis.

Tryptic peptides were analyzed on a Surveyor nanoLC system (Thermo) hyphenated to a LTQ-Orbitrap mass spectrometer (Thermo) as previously described.[1] Briefly, emitter, trap and analytical column (C18, 120 Å) were purchased from Nanoseparations (Nieuwkoop, The Netherlands) and mobile phases (A: 0.1% formic acid/H2O, B: 0.1% formic acid/ACN) were made with ULC/MS grade solvents (Biosolve). General mass spectrometric conditions were: electrospray voltage of 1.8-2.5 kV, no sheath and auxiliary gas flow, capillary voltage 40 V, tube lens voltage 155 V and ion transfer tube temperature 150 °C. Polydimethylcyclosiloxane (m/z = 445.12002) and dioctyl phthalate ions (m/z = 391.28429) from the milieu were used as lock mass. Some 10 µl of the samples was pressure loaded on the trap column for 5 min with a 10 µl/min flow and separated with a gradient of 35 min 5%–30% B, 15 min 30%–60% B, 5 min A at a flow of 300 µl/min split to 250 nl/min by the LTQ divert valve. Full MS scans (300–2000 m/z) acquired at high mass resolution (60,000 at 400 m/z, maximum injection time 1000 ms, AGC 106) in the Orbitrap was followed by three MS/MS fragmentations in the LTQ linear ion trap (AGC 5x103, max inj time 120 ms) from the three most abundant ions. MS/MS settings were: collision gas pressure 1.3 mT, normalized collision energy 35%, ion selection threshold of 750 counts, activation q = 0.25 and activation time 30 ms. Ions of $z < 2$ or unassigned were not analyzed and fragmented precursor ions were measured twice within 10 s and were dynamically excluded for 60 s. Data analysis was performed using Maxquant with acetylation (protein N term) and oxidation (M) as variable modifications. The false discovery rate was set at 1% and the peptides were screened against mouse proteome (Uniprot). Serine hydrolases that were identified in at least two repetitive experiments and for which at least 2 unique peptides were identified were considered as valid quantifiable hits.

Computational Chemistry

Docking of LEI104 in a previously reported homology model of DAGL-α was performed as described previously.[13] The structure of LEI104 was *in silico* modified to LEI105. The geometry was optimized using a fast Dreiding-like forcefield in the presence of the protein receptor. Depicted is one possible representative LEI105-like conformer.
The active conformation of OL-135 in the previously published co-crystal structure of FAAH with OL-135 (pdb: 2WJ2)[7] was *in silico* modified to the corresponding LEI105 heterocycle. The geometry was optimized using a fast Dreiding-like forcefield in the presence of the protein receptor. Depicted is one possible representative LEI105-like conformer.

DSI protocol

Horizontal slices (300 µm) of the hippocampus were obtained from male C57BL/6 mice (Harlan, the Netherlands) aged 14-19 days postnatal. Experiments were approved by the animal welfare committee of the University of Amsterdam. Animals were killed by decapitation, their brains quickly removed and placed in oxygenated (95% O_2 – 5% CO_2) ice cold (4 °C) adapted artificial cerebrospinal fluid (aACSF), containing in mM: 120 choline chloride, 3.5 KCl, 0.5 $CaCl_2$, 6 $MgSO_4$, 1.25 NaH_2PO_4, 25 D-glucose, 25 $NaHCO_3$). Slices were cut in aACSF on a vibratome (VT1200S, Leica, Germany) and placed for 30 min in regular ACSF (containing in mM: 120 NaCl, 3.5 KCl, 25 $NaHCO_3$, 25 D-glucose, 2.5 $CaCl_2$, 1.3 $MgSO_4$, 1.25 NaH_2PO_4) at 32 °C. Prior to recording, slices were kept at room temperature for at least one hour. Whole-cell voltage clamp recordings were made at 32 °C from the soma of CA1 pyramidal neurons (holding potential V_H = -80 mV). Recording pipettes were pulled from borosilicate glass (Science Products, Germany) and had a resistance of 2-3 MΩ when filled with pipette solution, containing in mM: 110 KGluconate, 30 KCl, 0.5 EGTA, 10 4-(2-hydroxyethyl)-1-piperazineethanesulfonic acid (HEPES), 4 Mg-ATP, 0.5 Na-GTP. Inhibitory postsynaptic currents (IPSCs) were evoked with a glass stimulus electrode (filled with ACSF) positioned in the stratum radiatum, close to the recorded neuron. With 200-µs biphasic stimulus pulses of half-maximal intensity the IPSCs were evoked every 5 sec. 20 µM 6-cyano-7-nitroquinoxaline-2,3-dione (CNQX) and 10 µM (2*R*)-amino-5-phosphonovaleric acid (AP5) were added to the ACSF to block glutamatergic synaptic currents and 5 µM carbachol to enhance inhibitory input. Recordings were made using an Axopatch 200B (Molecular Devices, USA) and in-house software running under Matlab (MathWorks, USA). Signals were low-pass filtered at 5 kHz and sampled at 10 kHz. Series resistance ranged from 5–15 MΩ and was compensated to ~65%. Voltage signals were corrected for liquid junction potential.

Stock solutions (10 mM) of LEI105 were made in dimethylsulfoxide (DMSO), which was diluted to the final concentration (10 µM) in ASCF. Recordings were made from CA1 neurons in slices that were pre-incubated with 10 µM LEI105 for at least 30 min; during the experiment this concentration was continuously present. Control experiments were performed on neurons recorded in slices pre-incubated with and in the continuous presence of 0.1% DMSO.

For each CA1 neuron IPSCs were evoked with 5 sec intervals during a 2-min baseline period, prior to the stimulus evoking depolarization-induced suppression of inhibition (DSI). The maximum amplitude of each IPSC was determined and the mean value of the IPCS amplitudes over this period was calculated and used to normalize the evoked synaptic response. DSI was induced by depolarizing the neuron from -80 to 0 mV for 5 sec. The normalized IPSC current amplitudes as a function of time were averaged and used for comparison between both treatments (Fig. 4B; control, n=18 neurons; LEI105, n=15 neurons). In control conditions the DSI protocol induced a short-lasting reduction of the

IPSC amplitude, which returned to baseline level with a single exponential time course. This recovery phase of the DSI response was fitted with a single exponential function and the time constant value obtained from this fit (τ = 34 sec) also correctly fitted the decay measured in the neurons treated with LEI105. DSI was then quantified as the relative reduction in the mean IPSC amplitude during the first 15 sec after DSI induction (Fig. 4C). DSI amplitudes were compared with Student's t-test, using $p<0.05$ to indicate a significant difference.

References

1. Katona, I.; Freund, T. F. *Annu. Rev. Neurosci.* **2012**, *35*, 529.
2. Devane, W. A.; Hanus, L.; Breuer, A.; Pertwee, R. G.; Stevenson, L. A.; Griffin, G.; Gibson, D.; Mandelbaum, A.; Etinger, A.; Mechoulam, R. *Science* **1992**, *258*, 1946.
3. Sugiura, T.; Kondo, S.; Sukagawa, A.; Nakane, S.; Shinoda, A.; Itoh, K.; Yamashita, A.; Waku, K. *Biochem. Biophys. Res. Commun.* **1995**, *215*, 89.
4. Mechoulam, R.; Ben-Shabat, S.; Hanus, L.; Ligumsky, M.; Kaminski, N. E.; Schatz, A. R.; Gopher, A.; Almog, S.; Martin, B. R.; Compton, D. R.; Pertwee R.G.; Griffin G.; Bayewitch M.; Barg J.; Vogel Z. *Biochem. Pharmacol.* **1995**, *50*, 83.
5. Gao, Y.; Vasilyev, D. V.; Goncalves, M. B.; Howell, F. V.; Hobbs, C.; Reisenberg, M.; Shen, R.; Zhang, M. Y.; Strassle, B. W.; Lu, P.; Mark, L.; Piesla, M. J.; Deng, K.; Kouranova, E. V.; Ring, R. H.; Whiteside, G. T.; Bates, B.; Walsh, F. S.; Williams, G.; Pangalos, M. N.; Samad, T. A.; Doherty, P. *J. Neurosci.* **2010**, *30*, 2017.
6. Di Marzo, V. *Nat. rev. Drug disc.* **2008**, *7*, 438.
7. Blankman, J. L.; Cravatt, B. F. *Pharmacol. Rev.* **2013**, *65*, 849.
8. Bisogno, T.; Howell, F.; Williams, G.; Minassi, A.; Cascio, M. G.; Ligresti, A.; Matias, I.; Schiano-Moriello, A.; Paul, P.; Williams, E. J.; Gangadharan, U.; Hobbs, C.; Di Marzo, V.; Doherty, P. *J. Cell Biol.* **2003**, *163*, 463.
9. Reisenberg, M.; Singh, P. K.; Williams, G.; Doherty, P. *Philos. Trans. R. Soc. Lond., B, Biol. Sci.* **2012**, *367*, 3264.
10. Tanimura, A.; Yamazaki, M.; Hashimotodani, Y.; Uchigashima, M.; Kawata, S.; Abe, M.; Kita, Y.; Hashimoto, K.; Shimizu, T.; Watanabe, M.; Sakimura, K.; Kano, M. *Neuron* **2010**, *65*, 320.
11. Appiah, K. K.; Blat, Y.; Robertson, B. J.; Pearce, B. C.; Pedicord, D. L.; Gentles, R. G.; Yu, X. C.; Mseeh, F.; Nguyen, N.; Swaffield, J. C.; Harden, D. G.; Westphal, R. S.; Banks, M. N.; O'Connell, J. C. *J. Biomol. Screen.* **2014**, *19*, 595.
12. Janssen, F. J.; Deng, H.; Baggelaar, M. P.; Allara, M.; van der Wel, T.; den Dulk, H.; Ligresti, A.; van Esbroeck, A. C. M.; McGuire, R.; Di Marzo, V.; Overkleeft, H. S.; van der Stelt, M. *J. Med. Chem.* **2014**, *57*, 6610.
13. Bisogno, T.; Mahadevan, A.; Coccurello, R.; Chang, J. W.; Allara, M.; Chen, Y.; Giacovazzo, G.; Lichtman, A.; Cravatt, B.; Moles, A.; Di Marzo, V. *Br. J. Pharmacol.* **2013**, *169*, 784.
14. Ortar, G.; Bisogno, T.; Ligresti, A.; Morera, E.; Nalli, M.; Di Marzo, V. *J. Med. Chem.* **2008**, *51*, 6970.
15. Hsu, K. L.; Tsuboi, K.; Adibekian, A.; Pugh, H.; Masuda, K.; Cravatt, B. F. *Nat. Chem. Biol.* **2012**, *8*, 999.

16. Niphakis, M. J.; Cravatt, B. F. *Annu. Rev. Biochem.* **2014**, *83*, 341.
17. Heal, W. P.; Dang, T. H.; Tate, E. W. *Chem. Soc. Rev.* **2011**, *40*, 246.
18. Liu, Y.; Patricelli, M. P.; Cravatt, B. F. *Proc. Natl. Acad. Sci. U. S. A.* **1999**, *96*, 14694.
19. Hoover, H. S.; Blankman, J. L.; Niessen, S.; Cravatt, B. F. *Bioorg. Med. Chem. Lett.* **2008**, *18*, 5838.
20. Yang, P. Y.; Liu, K.; Ngai, M. H.; Lear, M. J.; Wenk, M. R.; Yao, S. Q. *J. Am. Chem. Soc.* **2010**, *132*, 656.
21. Baggelaar, M. P.; Janssen, F. J.; van Esbroeck, A. C.; den Dulk, H.; Allara, M.; Hoogendoorn, S.; McGuire, R.; Florea, B. I.; Meeuwenoord, N.; van den Elst, H.; van der Marel, G. A.; Brouwer, J.; Di Marzo, V.; Overkleeft, H. S.; van der Stelt, M. *Angew. Chem. Int. Ed.* **2013**, *52*, 12081.
22. Fowler, C. J. *Fundam. Clin. Pharmacol.* **2006**, *20*, 549.
23. Boger, D. L.; Sato, H.; Lerner, A. E.; Hedrick, M. P.; Fecik, R. A.; Miyauchi, H.; Wilkie, G. D.; Austin, B. J.; Patricelli, M. P.; Cravatt, B. F. *Proc. Natl. Acad. Sci. U. S. A.* **2000**, *97*, 5044.
24. Pedicord, D. L.; Flynn, M. J.; Fanslau, C.; Miranda, M.; Hunihan, L.; Robertson, B. J.; Pearce, B. C.; Yu, X. C.; Westphal, R. S.; Blat, Y. *Biochem. Biophys. Res. Commun.* **2011**, *411*, 809.
25. van der Wel, T.; Janssen, F. J.; Baggelaar, M. P.; Deng, H.; den Dulk, H.; Overkleeft, H. S.; van der Stelt, M. *J. Lipid Res.* **2015, *56*, 927**.
26. Mileni, M.; Garfunkle, J.; DeMartino, J. K.; Cravatt, B. F.; Boger, D. L.; Stevens, R. C. *J. Am. Chem. Soc.* **2009**, *131*, 10497.
27. Bachovchin, D. A.; Ji, T.; Li, W.; Simon, G. M.; Blankman, J. L.; Adibekian, A.; Hoover, H.; Niessen, S.; Cravatt, B. F. *Proc. Natl. Acad. Sci. U. S. A.* **2010**, *107*, 20941.
28. Jung, K. M.; Astarita, G.; Thongkham, D.; Piomelli, D. *Mol. Pharmacol.* **2011**, *80*, 60.
29. Ohno-Shosaku, T.; Maejima, T.; Kano, M. *Neuron* **2001**, *29*, 729.
30. Wilson, R. I.; Nicoll, R. A. *Nature* **2001**, *410*, 588.
31. Hashimotodani, Y.; Ohno-Shosaku, T.; Kano, M. *J. Neurosci.* **2007**, *27*, 1211.
32. Hashimotodani, Y.; Ohno-Shosaku, T.; Maejima, T.; Fukami, K.; Kano, M. *Neuropharmacol.* **2008**, *54*, 58.
33. Hashimotodani, Y.; Ohno-Shosaku, T.; Tanimura, A.; Kita, Y.; Sano, Y.; Shimizu, T.; Di Marzo, V.; Kano, M. *J. Physiol.* **2013**, *591*, 4765.
34. Edwards, D. A.; Zhang, L. H.; Alger, B. E. *Proc. Natl. Acad. Sci. U. S. A.* **2008**, *105*, 8142.
35. Zhang, L. H.; Wang, M. N.; Bisogno, T.; Di Marzo, V.; Alger, B. E. *Plos One* **2011**, *6*.

36. Szabo, B.; Urbanski, M. J.; Bisogno, T.; Di Marzo, V.; Mendiguren, A.; Baer, W. U.; Freiman, I. *J. Physiol.* **2006**, *577*, 263.
37. Edwards, D. A.; Kim, J.; Alger, B. E. *J. Neurophysiol.* **2006**, *95*, 67.
38. Min, R.; Testa-Silva, G.; Heistek, T. S.; Canto, C. B.; Lodder, J. C.; Bisogno, T.; Di Marzo, V.; Brussaard, A. B.; Burnashev, N.; Mansvelder, H. D. *J. Neurosci.* **2010**, *30*, 2710.
39. Min, R.; Di Marzo, V.; Mansvelder, H. D. *Neuroscientist* **2010**, *16*, 608.
40. Alger, B. E.; Kim, J. *Trends Neurosci.* **2011**, *34*, 304.
41. Kunos, G.; Tam, J. *Br. J. Pharmacol.* **2011**, *163*, 1423.